Pharm Res (2011) 28:2920–2930
DOI 10.1007/s11095-011-0515-5

RESEARCH PAPER

Time-Correlated Single Photon Counting For Simultaneous Monitoring Of Zinc Oxide Nanoparticles And NAD(P)H In Intact And Barrier-Disrupted Volunteer Skin

Lynlee L. Lin • Jeffrey E. Grice • Margaret K. Butler • Andrei V. Zvyagin • Wolfgang Becker • Thomas A. Robertson • H. Peter Soyer • Michael S. Roberts • Tarl W. Prow

Received: 2 February 2011 / Accepted: 15 June 2011 / Published online: 30 June 2011
© Springer Science+Business Media, LLC 2011

ABSTRACT

Purpose There is a lack of relevant, non-animal alternatives for assessing exposure and toxicity of nanoparticle-containing cosmetics, e.g. sunscreens. Our goal was to evaluate time-correlated single photon counting (TCSPC) for simultaneous monitoring of zinc oxide nanoparticles (ZnO-NP) and the metabolic state of volunteer skin.

Methods We separated the fluorescence lifetime signatures of endogenous fluorophore signals (i.e. nicotinamide adenine dinucleotide phosphate, NAD(P)H and keratin) and the ZnO-NP signal using advanced TCSPC to simultaneously determine ZnO-NP penetration profiles and NAD(P)H changes in subjects with altered barrier function, including tape-stripped skin and in psoriasis or atopic dermatitis lesions.

Results We detected no ZnO-NP penetration into viable human skin in any group. ZnO-NP signal was significantly increased ($p < 0.01$) on the surface of tape-stripped and lesional skin after 4 and 2 h of treatment, respectively. Free NAD(P)H signal significantly increased in tape-stripped viable epidermis treated for 4 h of ZnO-NP compared to vehicle control. No significant NAD(P)H changes were noted in the lesional study.

Conclusion TCSPC techniques enabled simultaneous, real-time quantification of ZnO-NP concentration and NAD(P)H via non-invasive imaging in the stratum corneum and viable epidermis of volunteers.

L. L. Lin • J. E. Grice • M. S. Roberts • T. W. Prow
Therapeutics Research Centre, School of Medicine
Princess Alexandra Hospital, University of Queensland
Brisbane, Queensland, Australia

L. L. Lin • H. P. Soyer • T. W. Prow
Dermatology Research Centre, School of Medicine
Princess Alexandra Hospital, University of Queensland
Brisbane, Queensland, Australia

M. K. Butler
Australian Institute for Bioengineering & Nanotechnology
University of Queensland
Brisbane, Queensland, Australia

A. V. Zvyagin
Department of Physics, Centre of MQ Photonics
Macquarie University
Sydney, New South Wales, Australia

A. V. Zvyagin
Centre for Biophotonics and Laser Science
School of Physical Sciences, University of Queensland
Brisbane, Queensland, Australia

W. Becker
Becker & Hickl GmbH
Nahmitzer Damm 33
Berlin, Germany

T. A. Robertson • M. S. Roberts
Therapeutics Research Centre
School of Pharmacy & Biomedical Sciences
University of South Australia
Adelaide, South Australia, Australia

T. W. Prow (✉)
Therapeutics Research & Dermatology Research Centres
School of Medicine, Princess Alexandra Hospital
University of Queensland
Woolloongabba, Queensland 4102, Australia
e-mail: t.prow@uq.edu.au

KEY WORDS human skin · metabolism · multiphoton microscopy · sunscreen · zinc oxide nanoparticle

ABBREVIATIONS

AAS	atomic absorption spectroscopy
AU	arbitrary unit
CCT	caprylic/capric triglycerides
FLIM	fluorescence lifetime imaging microscopy
ICP-OES	inductively coupled plasma-optical emission spectroscopy
IRF	instrument response function
KDP	potassium di-hydrogen phosphate
MEP	multiphoton-excited photoluminescence
MPT	multiphoton tomography
MPT-FLIM	multiphoton tomography with fluorescence lifetime imaging microscopy
NAD(P)H	nicotinamide adenine dinucleotide phosphate
PBS	phosphate-buffered saline
SHG	second harmonic generation
TCSPC	time-correlated single photon counting
TEM	transmission electron microscope
TEWL	transepidermal Water Loss
Ti:Sa	titanium:sapphire
ZnO-NP	zinc oxide nanoparticles

INTRODUCTION

The European Union has committed to eliminating animal testing for cosmetics by 2013. Many organizations and research institutes have shown their support for this new policy and have been actively involved in developing new alternative methods (1–3). Particulate sunscreens range from micrometer to nanometer sizes. Sunscreens in both size ranges block harmful UV irradiation. Micrometer-sized sunscreens can block pores and can leave white residues. Nanoparticulate sunscreens overcome these issues and still protect skin from UV exposure (4). Sunscreens contain well-known UV filters such as zinc oxide (ZnO-NP) and titanium dioxide nanoparticles that protect the skin from UV damage (5,6). Recently, there has been concern over the safety of nanoparticles, especially in sunscreens. There has been considerable controversy over the penetration potential of topical nanoparticles (7–10). Although we and others have observed that ZnO-NP contained in sunscreen do not penetrate beyond the stratum corneum (11–14), more appropriate techniques are needed to assess nanoparticle penetration and biological effects in human studies.

Previous studies have used confocal microscopy to evaluate nanoparticle penetration in animal models and *in vitro* (for reviews see (7,15–17)). Barrier-disrupted skin has the potential for enhanced nanoparticle penetration (18). However, Samberg *et al.* recently showed that silver nanoparticles only penetrated into the uppermost layers of the stratum corneum after treatment for 2 weeks (19).

Current sunscreen formulations can also contain chemical enhancers that have the potential to increase ZnO-NP penetration into deeper layers of the skin. For instance, Kuo *et al.* (20) demonstrated, using multiphoton tomography (MPT), that chemical enhancers can increase the penetration of ZnO-NP into the stratum corneum of Balb/c mice. They concluded from the study that chemical enhancers can enhance the penetration of ZnO-NP either by increasing intercellular lipid fluidity or by extracting non-covalently bound amphiphilic lipid in the stratum corneum (20). However, statistical significance was not reported.

Unfortunately, keratin and ZnO-NP emission signals overlap spectrally, making this a confounding factor when trying to isolate the ZnO-NP signal in stratum corneum using the instrumentation described by Kuo *et al.* Another common confounder in nanoparticle penetration studies are the nanoparticle dissolution products; for example, ZnO-NP can solubilise within 2 h (21), and this material cannot be distinguished from the nanoparticles using some techniques. Gamer *et al.* (22), Cross *et al.* (11), and recently Gulson *et al.* (23) have investigated zinc penetration from ZnO-NP-containing sunscreens and found that the vast majority of zinc remains in the upper stratum corneum using quantitative methodologies that measure total zinc, e.g. inductively coupled plasma-optical emission spectroscopy (ICP-OES) and radio-labeled zinc.

MPT has the potential to compliment ICP-OES and similar techniques to provide particulate-only data. We and others have used optical techniques such as MPT to visualize ZnO-NP in human (24) and nude mouse skin (20). These mice (BALB/cAnN.Cg-Foxn1^{nu}/CrlNarl) lack hair due to defective hair follicles and also lack T-cells. NAD(P)H and keratin are the primary autofluorescent confounders in skin, and NAD(P)H levels can change with metabolism (25,26). Therefore, simultaneous quantification of nanoparticles and NAD(P)H offer the potential of penetration and metabolic data from the same optical biopsy.

The ZnO-NP penetration into skin can be quantified by isolating the fluorescence lifetime amplitude α_1% of ZnO-NP known as the ZnO multiphoton-excited photoluminescence (MEP) that is distinct from the autofluorescence of NAD(P)H. The MEP signal from ZnO-NP is not particularly strong, but is easily detectable with MPT. Our configuration takes images that are 210×210 μm^2 and ~1 μm in depth. Using this technique, the ZnO-NP signal within a single pixel (0.5×0.5×1 μm^3) can be detected if sufficient signal is present. Therefore, our hypothesis is that the MEP from ZnO-NP and NAD(P)H signals can be simultaneously quantified in volunteers by time-correlated single photon counting

(TCSPC)-enabled fluorescence lifetime imaging microscopy (FLIM).

This approach has the potential to facilitate toxicity assessment *in vivo* by quantifying the ZnO-NP signal present in an optical biopsy volume and NAD(P)H-related metabolic changes (25). We were limited to an *in vitro* standard curve because of the irregular three-dimensional structure and complex composition of skin. We found that our limit of detection was at the 1 mg/mL ZnO-NP MEP level at 30 μm below a glass cover slip, recognizing that the settings were tuned to simultaneously image ZnO-NP and NAD(P)H. The final goal was to examine nanoparticle penetration and metabolic effects of ZnO-NP-treated skin with altered barrier properties in volunteers.

MATERIALS AND METHODS

Subjects

All experiments conducted on human subjects were done with approval of Princess Alexandra Hospital Research Committee Approval No. 2007/197, administrated by the University of Queensland Human Ethics Committee. Our tape-strip, volunteer study involved a healthy subject with no history of skin disease. There were 8 subjects who had psoriasis/atopic dermatitis. Of those subjects, 5 had active psoriasis lesions, and the remainder had atopic dermatitis lesions.

Zinc Oxide Nanoparticles

ZinClear-S 60 CCT (ZnO-NP) (60% w/w) (Antaria, WA, Australia) consists of siliconate-coated ZnO-NP dispersed in caprylic/capric triglycerides (CCT) and was used for all studies.

Transmission Electron Microscopy

Samples containing ZnO-NP were rapidly frozen using a Leica EM PACT2 high-pressure freezer. Frozen samples were then cryosubstituted with 1% osmium tetroxide, 0.5% uranyl acetate and 5% H_2O in acetone at −80°C for 25 h before being gradually warmed to room temperature. Samples were subsequently infiltrated with Epon resin with the use of a microwave (Biowave, Pelco). Ultrathin sections were cut from polymerised blocks and examined with a JEOL 1010 transmission electron microscope at 100 keV.

Multiphoton Tomography

All multiphoton images were collected on a DermaInspect system (JenLab GmbH, Jena, Germany) with an ultra short pulsed mode-locked, 80 MHz, Titanium Sapphire MaiTai laser (Spectra Physics, Mountain View, CA, USA), which has a tuning range of 710–920 nm and an 85 femtosecond pulse width. The tomography system had an integrated TCSPC 830 detector to enable FLIM measurements. A Zeiss Plan-Neoflour oil-immersion 40×/1.30 objective lens was used. The excitation wavelength was 740 nm, and the average incident optical power was 21 mW at the rear of the objective. A band pass filter (350–450 nm) was used to select emission light ahead of the FLIM detectors. This detector consisted of a fast-response optical detector and photomultiplier tube to capture single photon events for FLIM analysis.

Transepidermal Water Loss (TEWL) and Tape-Stripping

TEWL for each test site was measured before and after tape-stripping, and after treatment with CCT vehicle solution or ZinClear-S 60 CCT. TEWL was not assessed in lesional studies. TEWL measurements were performed using AquaFlux AF200 closed chamber evaporimeter (Biox Systems Ltd., London, UK). AquaFlux V6.2 software was used to analyse the data. Tape-stripping was performed using 22 mm standard D-squame sampling discs while applying a consistent pressure of 225 g/cm^2 for 5 s for each tape strip using D-squame pressure instrument (Cuderm Corporation, Dallas, TX, USA).

In Vivo ZnO-NP Application

ZinClear-S 60 CCT stock solution was applied to a 2 cm^2 area of the subject's forearm at doses of 2 and 14 mg/cm^2 in tape-stripping and lesional studies, respectively. The treatment time was 4 and 24 h for the tape-stripping study and 2 h for the lesional studies. The test sites on subject's forearm were washed for 10 s and blotted dry to remove any loose material before and after treatment.

In Vitro Zinc Oxide Quantification

A total of 11 concentrations: 0, 0.05, 0.1, 0.5, 1, 5, 10, 50, 100, 150 and 200 mg/mL of ZnO-NP were prepared by stepwise dilution of a ZnO-NP stock preparation at 100 mg/mL, using Gilson 1000 positive displacement pipettes. Three sets of samples were prepared for each concentration. ZnO-NP standards were taken at a depth of 30 μm below the cover glass surface using MPT-FLIM. The FLIM images were analysed and the raw data exported. A standard curve was generated using the raw FLIM data and an exponential equation, $y = 0.6573e^{0.004\times}$, used to define the concentration of ZnO-NP of a given optical biopsy volume ($214\times214\times1$ μm^3). *In vitro*, the detection limit could be substantially lower than what we could measure *in vivo*. This is because of endogenous skin signals that override the ZnO-NP MEP. The endogenous signal obtained from

untreated skin was therefore defined as the limit of ZnO-NP MEP detection and not the values from the *in vitro* tests.

Extracting the MEP Signal from ZnO-NP in Human Skin

To extract the ZnO-NP MEP component from the recorded signal, we made use of the relative speed of the MEP signal of ZnO-NP amplitude (α_1%) compared to the endogenous autofluorescence because this does not change with the microenvironment, as does fluorescence lifetime (τ_1 and τ_2,). The MEP is an ultra-fast process, when compared to autofluorescence. TCSPC-FLIM data can be considered as an array of pixels, with each pixel containing a large number of time channels after the excitation pulse (27). To obtain fluorescence lifetime and amplitude data, the data points (i.e. the photon numbers in the time channels) were fitted with an appropriate model. The model function for a double-exponential decay profile is

$$f(t) = \alpha_1 e^{-t/\tau 1} + \alpha_2 e^{-t/\tau 2} \quad \text{with} \quad \alpha_1 + \alpha_2 = 1$$

with τ_1 and τ_2, and α_1 and α_2 being the lifetimes and the amplitudes of the fast and slow decay components. The lifetimes can change with microenvironment alterations, but, importantly, the amplitudes do not.

The model function, *f(t)*, is convoluted with the instrument response function, *IRF(t)*, to obtain a function *F(t)*. *F(t)* represents the shape of the signal that would be measured if the optical signal had the shape of the model function.

$$F(t) = f(t) * IRF(t) \quad (* \text{ is the convolution symbol})$$

F(t) is fitted to the measured data points, i.e. to the photon numbers in the consecutive time channels of each pixel of the image. The fit combines the ZnO-NP MEP component and possible fast fluorescence decay components in the fast decay component, $\alpha_1 e^{-t/\tau 1}$, within the model. Normal skin autofluorescence excited at 740 nm has α_1% values of 45–85. Values of α_1% above 90 are an indication that ZnO-NP MEP is detected.

FLIM Analysis

FLIM data were analysed with SPCImage 2.9.4 software. Two-component multi-exponential decay matrices were calculated for each image using an empirically defined

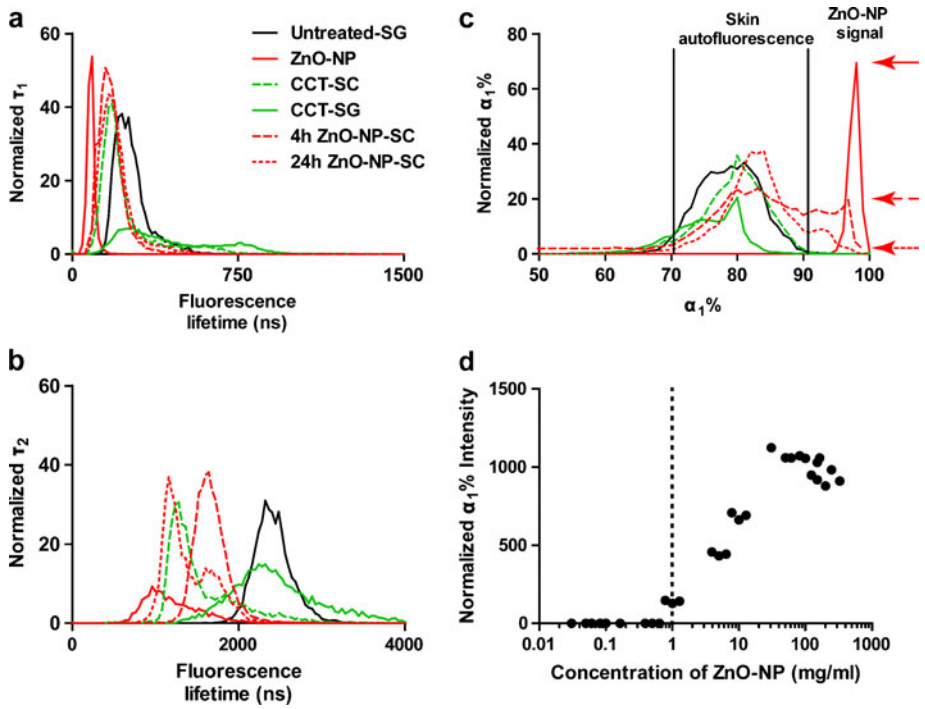

Fig. 1 Photonic characteristics of skin and ZnO-NP. (**a**–**c**) τ_1, τ_2 and α_1% histograms of the untreated stratum granulosum (Untreated-SG), CCT-treated stratum corneum after 24 h (CCT-SC), CCT-treated stratum granulosum after 24 h (CCT-SC), ZnO-NP alone (ZnO-NP), ZnO-NP on the stratum corneum after 4 h (4 h ZnO-NP-SC) and ZnO-NP on the stratum corneum after 24 h (4 h ZnO-NP-SC). (**c**) Distinct α_1 signals from skin autofluorescence and ZnO-NP MEP. The red arrows in (**c**) indicate maximal ZnO-NP intensity in ZnO-NP alone and after 4 and 24 h on the surface of the skin. (**d**) Generation of the *in vitro* ZnO-NP standard curve. Normalized α_1% 90–100 data were obtained from ZnO-NP solutions *in vitro*. The equation derived from the linear region (1.0–50.0 mg/mL) of this standard curve was $y = 0.6573e^{0.004x}$. The *dotted line* represents the mean value of normalized α_1% 45–85 from vehicle-treated stratum granulosum. The laser optical power was decreased to image ZnO-NP at 150.0 mg/mL and 200.0 mg/mL.

IRF. The region of interest was identified by the presence of visible cells within a z-plane and by excluding areas with furrows. The τ_1, τ_2, and α_1% numerical data were extracted from the regions of interest. This included the intensity-weighted pixel frequency and area (number of total pixels) for each region of interest. The normalized α_1% intensity was calculated by dividing the intensity-weighted pixel frequency by the area of the region of interest for each image in a z-stack. This was done separately for skin autofluorescence and ZnO-NP MEP using the α_1% cut-off levels above.

Statistical Analysis

The ZnO-NP results were analysed with nonparametric *t*-test to determine statistical significance, defined as $p<0.05$.

RESULTS

ZnO-NP and NAD(P)H Characteristics and ZnO-NP Standard Curve

FLIM analysis revealed the τ_1, τ_2 and α_1% signature of keratin in the stratum corneum, untreated NAD(P)H and keratin in the viable epidermis, and ZnO-NP. At 740 nm excitation, fluorescence lifetime profiles of keratin, untreated NAD(P)H and ZnO-NP overlapped, indicating that the ZnO-NP signal cannot be separated from the NAD(P)H using τ_1 and τ_2 profiles under these conditions (Fig. 1a and b).

The τ_1 and τ_2 cannot be used to identify the presence of ZnO-NP due to the capacity for these lifetimes to shift (Fig. 1a and b) depending on the microenvironment. The keratin and untreated NAD(P)H fluorescence lifetime signal amplitude (α_1%) ranges from 55 to 95 and ZnO-NP from 90 to 100. The peak at 90–100 represents the ultrafast MEP from ZnO-NP. In contrast, the α_1% from untreated NAD(P)H in stratum granulosum exists as a relatively slower fluorescence signal and not MEP emission. The normalized α_1% data shown on the y-axis correspond to the intensity of the signal. The ZnO-NP signal from ZnO-treated skin at 4 h decreased from 70 to 20, and a further decrease to <5 of the normalized value at 24 h (Fig. 1c, red arrows) compared to ZnO-NP alone. Vehicle-only (i.e. CCT) treated and untreated skin showed no ZnO-NP signal (α_1% 90–100), shown in Fig. 1c. Likewise, CCT application did not change the τ_1 or τ_2 profiles. The NAD(P)H α_1/α_2 ratios in untreated (3.5 ± 0.4) and CCT-treated (3.3 ± 0.2) skin were almost identical after 24 h treatment in the stratum granulosum.

Due to the nature of α_1% photonic property, we have used the α_1% intensity signal from ZnO-NP to develop the standard curve as shown in Fig. 1d. A standard curve

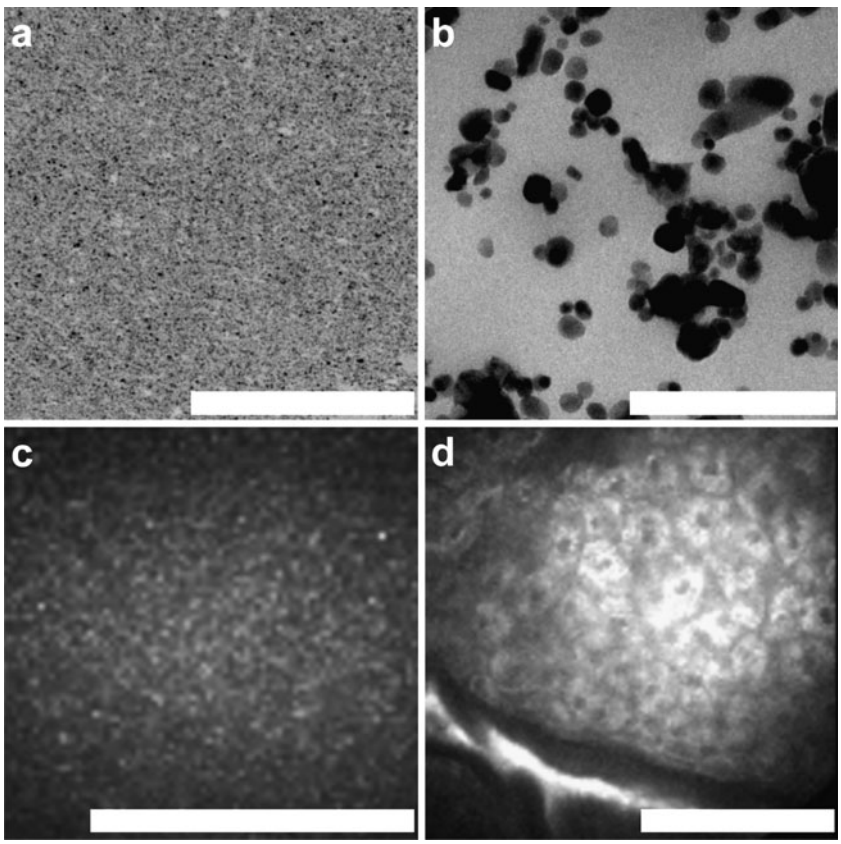

Fig. 2 TEM images of ZnO-NP and MPM ZnO-NP and the viable epidermis. TEM images of 1 mg/mL ZnO-NP show the 35 nm nanoparticles at low (**a**) and high magnification (**b**). MPT intensity image of a 1 mg/mL ZnO-NP solution (**c**) and untreated volunteer viable epidermis (**d**). The MPT images in (**c** and **d**) were taken with 740 nm excitation. The *scale bars* indicate 10 μm (**a**), 200 nm (**b**), and 50 μm (**c** and **d**).

consisting of 11 concentrations of ZnO in CCT (ranging from 0 to 200 mg/mL) was used to quantify the concentration of ZnO-NP in the human volunteer's skin (Fig. 1d). The concentration of a given optical biopsy volume ($214\times214\times1\ \mu m^3$) can be determined using the equation $y = 0.6573e^{0.004\times}$, derived from the standard curve. The skin autofluorescence signals in the stratum corneum and viable epidermis limit the detection of low ZnO-NP MEP levels when excited at 740 nm; therefore, the lower detection limit of ZnO-NP MEP signal was dictated by these autofluorescence background signals at the 1 mg/mL ZnO-NP MEP level.

We investigated the morphology and aggregation state of dispersed ZnO-NP in CCT vehicle solution using TEM. The nanoparticles used in this study ranged from 10 to 50 nm in diameter (Fig. 2a and b). The surface charge of similar sized ZnO-NP is 20–60 mV in water at physiological pH (28). Fig. 2c and d show MPT intensity images of ZnO-NP alone and untreated volunteer skin at the stratum granulosum level.

The photonic characteristics ZnO-NP-treated and untreated volunteer skin can also be represented in FLIM pseudocolored multiphoton images. The pseudocolored images in Fig. 3 depict the presence of different signals at α_1% ranging from 85–100. Blue indicates keratin and/or NAD(P)H signals (α_1%=85−90) in the stratum corneum and stratum granulosum, while green-red indicates ZnO-NP MEP (α_1%=90−100).

Analysis of the ZnO-NP Signal and NAD(P)H Lifetime Changes in Intact and Tape-Stripped Volunteer Skin

60% ZinClear-S 60 CCT, which is an active ingredient in many sunscreens containing 10–50 nm of ZnO-NP, was

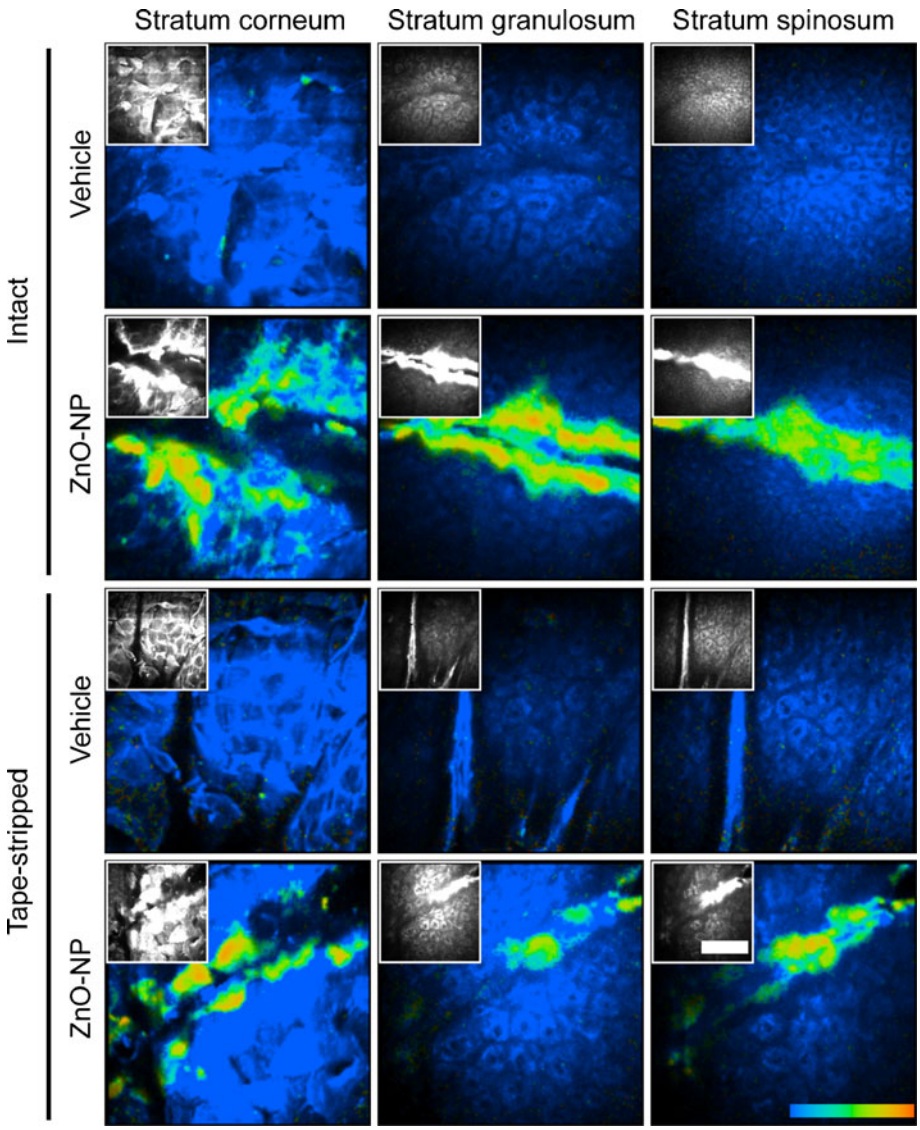

Fig. 3 *In vivo* multiphoton images of intact and tape-stripped volunteer skin at different depths after 24 h treatment. Each image is $214\times214\times1\ \mu m^3$. These colour images depict the autofluorescence as blue (α_1% 0–85) and ZnO-NP as green-red (α_1% 90–100) in volunteer skin. The *gray scale* insets are intensity-only images. All *bars* indicate 100 μm. The *colour scale bar* represents α_1% 85–100, blue-red.

used in the *in vivo* experiments. TEWL measurements showed intact subject skin prior to tape-stripping at a TEWL range between 18.4±2.0 g/m^{2}h. The skin TEWL range increased to 48.8±10.1 g/m^2 h after 20× tape-stripping.

Pseudocolored multiphoton images revealed no ZnO-NP signal in skin treated with CCT solution vehicle alone (Fig. 3, vehicle). After ZnO-NP treatment, the ZnO-NP signal was localized on stratum corneum and in furrows of both intact and tape-stripped skin, but no ZnO-NP signal was observed in the viable epidermis (Fig. 3, ZnO-NP).

In the stratum corneum, we observed a decrease in the keratin signal amplitude (normalized α_1% 45–85, shown in AU) of intact skin from 407.8±142.4 to 221.8±9.0 after 4 h of treatment with ZnO-NP. However, the stratum corneum keratin signal increased from 221.8±9.0 in the 4 h ZnO-NP-treated group to 355.3±60.3 after 24 h ZnO-NP treatment (Fig. 4a). Similar to intact skin, no ZnO-NP signal was detected in CCT-treated, tape-stripped skin. Higher levels of ZnO-NP signal were detected in the remaining stratum corneum of tape-stripped skin than intact skin, 402.8±55.6 and 156.9±83.7, respectively after 4 h post treatment. The calculated ZnO-NP concentration of tape-stripped and intact skin after 4 h was 34.03±15.13 mg/mL and 5.16±3.85 mg/mL, respectively. Likewise, we recorded less keratin signal in the stratum corneum of tape-stripped skin than intact skin, to 221.8±9.0 and 95.4±45.2, respectively (Fig. 4a and b). There was no significant change in level of keratin signal in ZnO-NP-treated, tape-stripped stratum corneum after 4 h. However, we observed a significant increase ($p=0.039$) in the keratin signal within the tape-stripped, stratum corneum with 4 to 24 h ZnO-NP treatment (Fig. 4b). Interestingly, only a relatively minute ZnO-NP signal was detected in the stratum corneum of tape-stripped skin after 24 h, compared to 4 h (8.8±3.3 *vs.* 402.8±55.6, $p=0.002$) (Fig. 4b). This suggests that the ZnO-NP may be dissolving throughout the 24 h treatment window.

There was no difference in NAD(P)H/keratin levels in intact, stratum granulosum as seen in Fig. 4c. However, we observed a significant increase, $p=0.018$, in NAD(P)H/keratin signal in tape-stripped stratum granulosum after 4 h post treatment with ZnO-NP compared to vehicle-only treated skin (Fig. 4d). This trend was also observed for stratum spinosum as shown in Fig. 4e–f. There was little to no detectable ZnO-NP signal within our detection capability across all treatment groups in stratum granulosum and

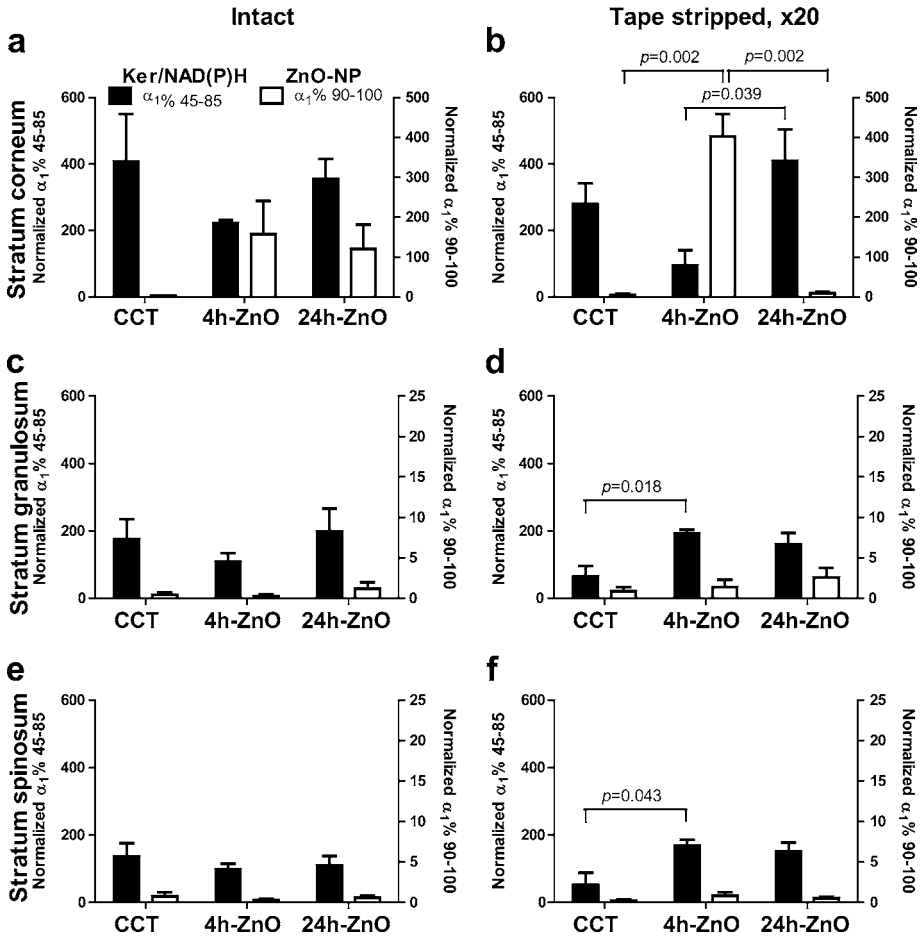

Fig. 4 Quantification of keratin/NAD(P)H signals, at α_1% 45–85, and the ZnO-NP signal, at α_1% 90–100, in intact, tape-stripped (20 strips) volunteer skin. *p* values from nonparametric *t*-tests are shown where $p<0.05$.

stratum spinosum of both intact skin and tape-stripped skin, suggesting no penetration enhancement of ZnO-NP into viable epidermis by tape-stripping within our detection range (Fig. 4c–f). Statistical analysis revealed no statistically significant penetration enhancement with tape-stripping. Perhaps more aggressive removal of the stratum corneum could lead to different outcomes.

Quantification of ZnO-NP Penetration and Metabolic State In Volunteers With Psoriatic and Atopic Dermatitis Lesions

ZnO-NP applied to the surface of lesional skin was immediately evident upon MTP-FLIM imaging (Fig. 5). In contrast to the non-lesional skin, there were fewer furrows in the lesional areas. The ZnO-NP signal was strong in the thick stratum corneum of the lesional tissue. However, the ZnO-NP signal abruptly stopped just before the stratum granulosum layer (Fig. 5, middle column) and was absent in the deeper layers of lesional skin. The penetration profiles of ZnO-NP (α_1% 90–100) are shown for non-lesional and lesional skin in Fig. 6a and b, respectively, from areas without furrows (epidermal plateaus). ZnO-NP concentrations were found to be highly variable in the stratum corneum directly above viable epidermal plateaus (−5 μm) in both non-lesional (2.98 ± 2.05 mg/mL) and lesional skin (2.59 ± 1.86 mg/mL) treated with sunscreen (Fig. 6a and b, respectively). Only the lesional skin showed a very significant ($p > 0.005$) difference in ZnO-NP concentrations compared to untreated skin. There was no ZnO-NP signal within our detection range in the superficial viable epidermis (0 μm)

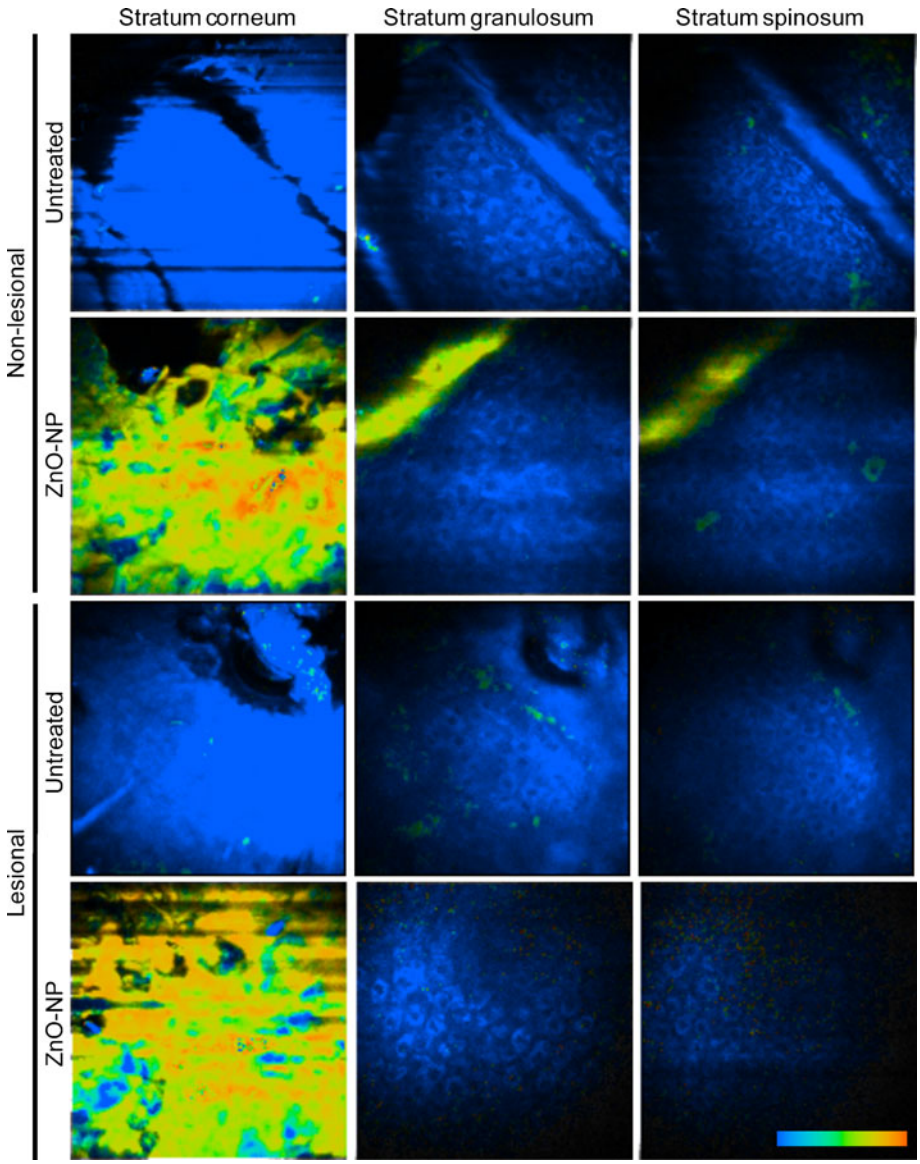

Fig. 5 *In vivo* multiphoton images of non-lesional and lesional volunteer skin of different depths after 2 h treatment with ZnO-NP. Each image is 214 × 214 × 1 μm^3. These colour images depict the autofluorescence as blue (α_1% 0–85) and ZnO-NP as green-red (α_1% 90–100) in volunteer skin. All *bars* indicate 100 μm. The *colour scale bar* represents α_1% 85–100, blue-red.

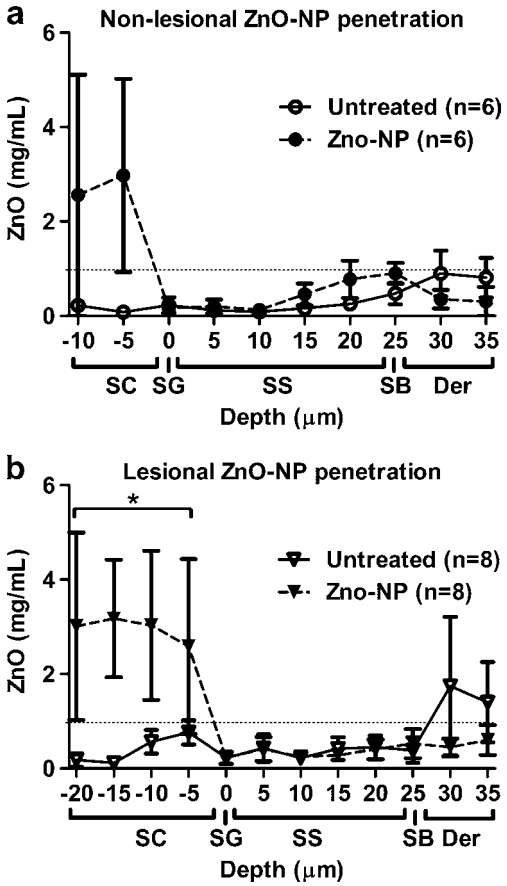

Fig. 6 ZnO-NP penetration profiles, excluding furrows, in non-lesional (**a**) and lesional (**b**) volunteer skin. ZnO-NP signal was quantified using α_1% 90–100 and normalized to the region of interest area. *Asterisk* indicates p value of >0.005 when compared to untreated skin.

of ZnO-NP-treated non-lesional, lesional skin, untreated non-lesional and lesional sites. In Fig. 6b, there is an increased signal from >25 μm in the untreated group. This is likely to be the SHG signal from collagen in the papillary dermis. Second harmonic generation from collagen is a confounding factor that restricts the use of this methodology to the viable epidermis. This is due to the overlapping FLIM characteristics of SHG and MEP that cannot be separated.

DISCUSSION

We have shown for the first time that TCSPC enables non-invasive, simultaneous ZnO-NP quantification and NAD(P)H lifetime analysis in volunteers with altered barrier function. Vehicle-only controls did not show any ZnO-NP signal. ZnO-NP signal was detected in the stratum corneum of both intact and tape-stripped skin treated with ZnO-NP. Interestingly, we found significantly higher ZnO-NP signal in tape-stripped skin compared to intact skin after 4 h of exposure. The concentrations of detectable ZnO-NP in intact and tape-stripped stratum corneum were 5.16 ± 3.85 and 34.03 ± 15.13 mg/mL at 4 h, and 2.69 ± 1.41 and below 1.00 mg/mL at 24 h, respectively. We are the first to show no enhanced penetration nor any significant ZnO-NP signal within our detection capability in the viable epidermis of tape-stripped skin treated with ZnO-NP. Likewise, this is the first study to show no detectable ZnO-NP penetration into the viable epidermis of ZnO-NP treated psoriasis/atopic dermatitis lesions; however, there was a significant increase ($p<0.01$) in the ZnO-NP levels in the stratum corneum when compared to treated non-lesion sites after 2 h of treatment. The reduced exposure time, from 4 to 2 h, in the psoriasis/atopic dermatitis experiments is a limitation of this study that will be addressed in our future work involving ZnO-NP penetration in compromised volunteer skin.

A recent publication by Bian *et al.* shows that the *in vitro* dissolution of zinc nanoparticles reaches equilibrium within 2 h in aqueous solution (21). This supports our finding in Fig. 1c, where we show a substantial decrease in ZnO-NP signal after 4 and more so at 24 h treatment (Fig. 1c, red arrows). We are the first to explore a time course study on ZnO-NP penetration with MPT in volunteers.

The issue of nanoparticle penetration involves many variables, including skin, formulation, detection limits, nanoparticle surface properties and nanoparticle dissolution kinetics. We have recently described the penetration of quantum dots, similar in size to the ZnO-NP in human skin, where we investigated surface coating, pH and barrier properties of the skin (29). We found that the skin barrier was the primary factor determining nanoparticle penetration into human skin, with pH and surface coating only having minor effects. The rapid dissolution of ZnO-NP and the stability of quantum dots could contribute to the observation that ZnO-NP penetrates tape-stripped human skin to a lesser degree than do quantum dots.

Studies by Gulson *et al.*, Cross *et al.* and Gamer *et al.* found that insignificant quantities of zinc penetrate beyond stratum corneum in humans, human skin or porcine skin treated with sunscreens (11,22,23). These studies were unable to conclude if the presence of zinc was due to dissolved zinc or ZnO-NP (11,22,23). These data are congruent with our findings, recognizing that we evaluated nanoparticle specific signals and the referenced studies evaluated total zinc.

Kuo *et al.* and Zvyagin *et al.* demonstrated the degree of ZnO-NP that penetrated into skin of the mouse models and human subjects using photonic intensity (20,24) and were largely consistent with our results. The technique developed in our study can complement these approaches by removing confounding autofluorescent signals from the skin.

The previously mentioned studies all focused on the penetration of nanoparticles and not metabolic effects. Using FLIM analysis of NAD(P)H, we have uncovered several NAD(P)H effects of topical ZnO-NP treatment in human skin, shown in Fig. 4. However, the majority of these changes were not statistically significant and only represent trends. We found slight increases in autofluorescent signals (keratin/NAD(P)H) in tape-stripped skin that tended to increase with treatment time in the stratum granulosum. However, in all the other cases examined, there were no other consistent trends or changes in NAD(P)H lifetime or signal in the viable epidermis. We did observe an increased autofluorescent signal from the stratum corneum treated with ZnO-NP for 4 h, but this was not found at 24 h. These data suggest that, under these conditions, the ZnO-NP did not have a detectable effect on NAD(P)H in the viable epidermis of treated volunteers.

There are several limitations to the approach described here. First, it is known that ZnO-NP MEP and SHG emitted from collagen found within connective tissues cannot be separated, but SHG discrimination is not a problem for measurements in the viable epidermis and stratum corneum, as collagen is located only in deeper skin layers (i.e., the dermis). Therefore, the use of the MEP signal to quantify ZnO-NP is limited to the superficial skin and excludes the dermis. Another limitation is that only ZnO-NP concentrations can be quantified and not other forms of zinc (e.g. solubilised ZnO or zinc ions) and that the standard curve was derived *in vitro* rather than *in vivo*. Simultaneous ZnO-NP and keratin/NAD(P)H analysis is also limited by the need to balance excitation laser power with detector gain. Therefore, while the parameters are adjusted to capture NAD(P)H fluorescence, a decreased range of detectable ZnO-NP results.

CONCLUSION

In conclusion, TCSPC has the potential for enabling studies on exposure and metabolic consequences of nanoparticle-containing topical products in human subjects without the need for painful biopsies or destructive analysis. Our studies showed that ZnO-NP signal was strongest in furrows, and this signal was weakest 24 h after treatment. Our volunteer studies demonstrated that there was increased ZnO-NP signal from the stratum corneum of disrupted and lesional skin, but there was no ZnO-NP signal within our detection limits in the viable epidermis of any group tested. This is the first time that a systematic study has been done to non-invasively assess ZnO-NP penetration and metabolic state in volunteers with tape-stripped skin and in treated psoriatic/atopic dermatitis lesions.

ACKNOWLEDGMENTS & DISCLOSURES

We would like to thank the National Health and Medical Research Council of Australia (ID# 569694) and the United States Air Force Asian Office of Aerospace Research and Development for funding. We also thank Corinne Yoong for recruiting volunteers for the lesion studies.

REFERENCES

1. DIRECTIVE 2003/15/EC OF THE EUROPEAN PARLIAMENT AND OF THE COUNCIL. Official Journal of the European Union 2003;46:26–35, .
2. Regulation (EC) No 1223/2009 of the European Parliament and of the Council of 30 November 2009 on cosmetic products Official Journal of the European Union. 52:59–209 (2009).
3. Ruet Rossignol M. The 7th Amendment to the Cosmetics Directive. Altern Lab Anim. 2005;33 Suppl 1:19–20.
4. Robertson TA, Sanchez WY, Roberts MS. Are commercially available nanoparticles safe when applied to the skin? J Biomed Nanotechnol. 2010;6:452–68.
5. Ahmed AH, Soyer HP, Saunders N, Boukamp P, Roberts MS. Non-melanoma skin cancers. Drug Discovery Today: Disease Mechanisms: Skin diseases. 2008;5:e55–62.
6. Leiterand U, Garbe C. Epidemiology of melanoma and non-melanoma skin cancer–the role of sunlight. Adv Exp Med Biol. 2008;624:89–103.
7. Monteiro-Rivierеand NA, Riviere JE. Interactions of nanomaterials with skin: Aspects of absorption and biodistribution. Nanotoxicology. 2009;3:188–95.
8. Nohynek GJ, Lademann J, Ribaud C, Roberts MS. Grey goo on the skin? Nanotechnology, cosmetic and sunscreen safety. Crit Rev Toxicol. 2007;37:251–77.
9. Singhand S, Nalwa HS. Nanotechnology and health safety–toxicity and risk assessments of nanostructured materials on human health. J Nanosci Nanotechnol. 2007;7:3048–70.
10. Sternand ST, McNeil SE. Nanotechnology safety concerns revisited. Toxicol Sci. 2008;101:4–21.
11. Cross SE, Innes B, Roberts MS, Tsuzuki T, Robertson TA, McCormick P. Human skin penetration of sunscreen nanoparticles: *In-vitro* assessment of a novel micronized zinc oxide formulation. Skin Pharmacol Phys. 2007;20:148–54.
12. Durand L, Habran N, Henschel V, Amighi K. *In vitro* evaluation of the cutaneous penetration of sprayable sunscreen emulsions with high concentrations of UV filters. Int J Cosmet Sci. 2009;31:279–92.
13. Newman MD, Stotland M, Ellis JI. The safety of nanosized particles in titanium dioxide- and zinc oxide-based sunscreens. J Am Acad Dermatol. 2009;61:685–92.
14. Roberts MS, Roberts MJ, Robertson TA, Sanchez W, Thorling C, Zou Y, *et al*. *In vitro* and *in vivo* imaging of xenobiotic transport in human skin and in the rat liver. J Biophotonics. 2008;1:478–93.
15. Kortingand HC, Schafer-Korting M. Carriers in the topical treatment of skin disease. Handb Exp Pharmacol :435–468 (2010).
16. Prow TW, Grice JE, Lin LL, Faye R, Butler MK, Becker W, Wurme EMT, Yoong Y, Robertsona TA, Soyer HP, Roberts MS. Nanoparticles and Microparticles for Skin Drug Delivery. Adv Drug Del Rev:In press. (2011).
17. Schneider M, Stracke F, Hansen S, Schaefer UF. Nanoparticles and their interactions with the dermal barrier. Dermatoendocrinol. 2009;1:197–206.

18. Zhangand LW, Monteiro-Riviere NA. Assessment of quantum dot penetration into intact, tape-stripped, abraded and flexed rat skin. Skin Pharmacol Phys. 2008;21:166–80.
19. Samberg ME, Oldenburg SJ, Monteiro-Riviere NA. Evaluation of silver nanoparticle toxicity in skin *in vivo* and keratinocytes *in vitro*. Environ Health Perspect. 2010;118:407–13.
20. Kuo TR, Wu CL, Hsu CT, Lo W, Chiang SJ, Lin SJ, *et al.* Chemical enhancer induced changes in the mechanisms of transdermal delivery of zinc oxide nanoparticles. Biomaterials. 2009;30:3002–8.
21. Bian SW, Mudunkotuwa IA, Rupasinghe T, Grassian VH. Aggregation and Dissolution of 4 nm ZnO Nanoparticles in Aqueous Environments: Influence of pH, Ionic Strength, Size, and Adsorption of Humic Acid. Langmuir (2011).
22. Gamer AO, Leibold E, van Ravenzwaay B. The *in vitro* absorption of microfine zinc oxide and titanium dioxide through porcine skin. Toxicology *in Vitro*. 2006;20:301–7.
23. Gulson B, McCall M, Korsch M, Gomez L, Casey P, Oytam Y, *et al.* Small amounts of zinc from zinc oxide particles in sunscreens applied outdoors are absorbed through human skin. Toxicol Sci. 2010;118:140–9.
24. Zvyagin AV, Zhao X, Gierden A, Sanchez W, Ross JA, Roberts MS. Imaging of zinc oxide nanoparticle penetration in human skin *in vitro* and *in vivo*. J Biomed Opt. 2008;13:064031.
25. Sanchez WY, Prow TW, Sanchez WH, Grice JE, Roberts MS. Analysis of the metabolic deterioration of ex vivo skin from ischemic necrosis through the imaging of intracellular NAD(P)H by multiphoton tomography and fluorescence lifetime imaging microscopy. J Biomed Opt. 2010;15:046008.
26. Ying W. NAD+/NADH and NADP+/NADPH in cellular functions and cell death: regulation and biological consequences. Antioxid Redox Signal. 2008;10:179–206.
27. Becker W. Advanced time-correlated single photon counting techniques. Berlin: Springer; 2005.
28. Berg JM, Romoser A, Banerjee N, Zebda R, Sayes CM. The relationship between pH and zeta potential of similar to 30 nm metal oxide nanoparticle suspensions relevant to *in vitro* toxicological evaluations. Nanotoxicology. 2009;3:276–83.
29. Prow TW, Monteiro-Riviere NA, Inman AO, Grice JE, Chen X, Zhao X, Sanchez WH, Gierden A, Kendall MA, Zvyagin AV, Erdmann D, Riviere JE, Roberts MS. Quantum dot penetration into viable human skin. Nanotoxicology 2011.